Comparison of EUV spectral and ion emission features from laser-produced Sn and Li plasmas

R. W. Coons, D. Campos, M. Crank, S. S. Harilal, and A. Hassanein
School of Nuclear Engineering, and Center for Materials Under Extreme Environment,
Purdue University, West Lafayette, Indiana, 47907, USA

ABSTRACT

Planar slabs of pure Sn and Li were irradiated with 1064 nm, 9 ns Nd:YAG laser pulses. The resulting plasmas were evaluated with an absolutely calibrated extreme ultraviolet (EUV) power tool, a transmission grating spectrograph, a pinhole camera, and a Faraday cup. These diagnostic tools have allowed us to determine EUV conversion efficiency (CE), EUV spectral emission features, EUV-emitting plasma size, and the kinetic energies and fluxes of ions at various laser intensities for both Sn and Li plasmas. The maximum estimated CE values for Li and Sn plasmas are 1 ± 0.1 % and 2 ± 0.2 %, respectively. The Li^{2+} Lyman-α line and Sn^{8-13+} lines generate the in-band emissions of Li and Sn. The intensity of Li^{2+} lines was found to increase with laser intensity. However, the Sn unresolved transmission array (UTA) showed remarkable changes with at higher laser intensities, including the appearance of a spectral dip. EUV plasma images showed that Sn plasmas take on a conical shape, as opposed to the hemispherical shape of Li plasmas. Ion debris analysis showed the kinetic energies for Li ions are less than that of Sn ions under similar conditions. Moreover, the kinetic spread of Li ions has been found to be narrower compared to the kinetic energy distribution of the Sn ions. We also compared the ion flux emitted by Sn and Li plasmas.

Keywords: EUV lithography, laser-produced plasma, plasma diagnostics, emission spectroscopy

1. INTRODUCTION

Much research has been conducted on generating laser-produced plasma(LPP) sources emitting at 13.5 nm [1-5] from a number of different target materials, including Sn [2, 6], Xe [7], and Li [8]. The essential requirements of a LPP source for extreme ultraviolet lithography (EUVL) are a high CE (conversion from laser energy to 13.5 nm with 2% bandwidth) with minimum debris generation, as to prevent damage to the multi-layered mirrors (MLMs) which are critical to EUVL manufacturing systems.

The EUV CE from a LPP plasma strongly depends on various laser parameters (wavelength [5], pulse width [4], spot size [4, 9], power density [10, 11], etc.) and target specifications (mass density [10, 12], target geometry [11, 13], etc.) Previous studies have clearly demonstrated that Sn plasmas are more efficient at generating in-band EUV radiation than Li or Xe plasmas. Depending upon the experimental parameters, reported Sn plasma CE values varied from 2-5% [4, 9, 14], and from 1-2% [8, 14, 15] and 0.3-0.8% [7, 16] for Li and Xe, respectively. Apart from CE, the cleanness of the LPP source is extremely important for their use in EUVL. The LPP emits debris in the form of energetic ions, atoms, and molten droplets, which are difficult to control [6, 17-19]. This ablated target material vapor-deposits itself on various components within a direct line-of-sight of the plasma, including the surface of the MLM, which causes degradation in mirror reflectivity. Additional reflectivity losses are brought on through the ion-induced sputtering of the mirror itself. Previous studies showed that along with fast moving ions, Sn neutrals also contribute a significant reduction in MLM reflectivity [20]. Several ion and atom debris mitigation schemes have been proposed [6, 17, 21, 22], although they cannot completely mitigate the additional damage from neutrally-charged debris. Because of its negative effects, ion and neutral debris must be further characterized, so that effective debris mitigation schemes can be implemented.

In this paper, we compared the EUV emission features, as well ion and atom debris, emanating from two efficient LPP target sources (Li and Sn) at 13.5 nm. We also investigated the effect of laser spot size and laser power density on the CE and the EUV spectral features of both Li and Sn plasmas. The ion fluence and ion energies for each material were measured, along with images and emission spectra of their plasmas.

Extreme Ultraviolet (EUV) Lithography, edited by Bruno M. La Fontaine, Proc. of SPIE Vol. 7636,
763636 · © 2010 SPIE · CCC code: 0277-786X/10/$18 · doi: 10.1117/12.848318

2. METHODOLOGY

A schematic of the experimental setup is given in Figure 1. For producing plasmas, 1064 nm, 9 ns (Full Width Half Maximum (FWHM)) pulses from a Nd:YAG laser were used. Planar slabs of pure Sn and Li were mounted to a servo-motor controlled XYZ translation stage inside of a stainless steel high-vacuum chamber, which was evacuated with a turbomolecular pump to a pressure < 10^{-6} Torr. The focusing lens was mounted on a micrometer-controlled translation stage, allowing for fine-tuning of the laser spot size. The target was translated between shots to refresh the target surface, and to mitigate the effects of target cratering. This new surface was exposed to a low energy "cleaning pulse" to ablate any oxide layers from the target before each measurement.

The CE of the incident pulse energy to 13.5 nm radiation was measured with an EUV power tool, which consists of two Zr filters and a Mo/Si MLM to reflect the incoming plasma light into an absolutely calibrated photodiode. The photodiode signal is then displayed and recorded on an oscilloscope. The emission spectra of Li and Sn plasmas were recorded using a transmission grating spectrometer (TGS). The TGS utilizes a silicon nitride diffraction grating with a 10,000 lines/mm resolution. The time-integrated spectra were then recorded with an EUV sensitive CCD camera. EUV images of the plasma were obtained by mounting a 50 μm pinhole at the end of a 49.2 cm tube, placed 51 mm from the target point, creating a simple pinhole camera with a magnification of 11. The pinhole camera employs a Zr filter which filters radiation in the 7-15 nm wavelength range.

The fluence and kinetic energy of the plasma ions were measured with a Faraday cup (FC) mounted inside the chamber, 17 cm from the target point at a 12° angle from the plane of the beam. The FC was biased with a DC power supply to the optimized potential difference of -31 V. The ion current was measured by acquiring the voltage signal across a load resistor, and was viewed with a 350 MHz digital phosphor oscilloscope.

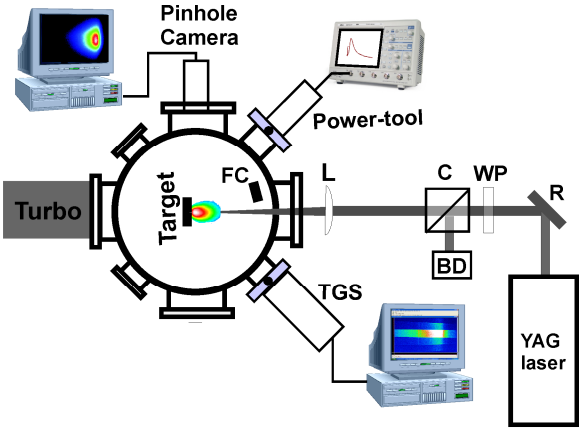

Figure 1. Schematic of experimental setup. Optical components include a polarizing cube (C), a half-wave plate (WP), focusing lenses (L), reflector (R). (FC, Faraday cup; BD, beam dump; TGS, transmission-grating spectrograph).

3. RESULTS AND DISCUSSIONS

LPPs are a highly transient phenomena, whose properties are strongly material and temperature dependent. The spectral emission features of the plasmas are dependent on their temperature and density. Typically, LPPs emit strongly in the EUV spectral region when heated to 20-40 eV [23]. The intensity of the laser beam determines the temperature of the plasma, through the degree of excitation of its constituent atoms. Along with spectral emission, the laser intensity also affects the kinetics of neutral and ion particles emanating from the plasma. Earlier reports showed that the average charge state of the Sn plasma is ~ 11 when the Sn plasma is heated to ~ 30 eV, which is the optimal condition for maximum CE [24]. Increasing the laser intensity leads to the production of highly charged ions with higher kinetic energies, which are more dangerous for the collector mirror in the EUV setup. We used a suite of diagnostic tools to investigate spectral and ion emission from Sn and Li produced plasmas, including in-band CE measurement, EUV spectroscopy, EUV pinhole imaging, and FC ion analysis. These studies are very useful for understanding suitable EUV emission conditions from Sn and Li plasmas, as well the nature of the debris they emit. Since Sn and Li are considered to

be potential targets for a LPP source, a comparison between the spectral and ion emissions with identical experimental parameters will be extremely useful for the ongoing development of EUV light sources.

3.1 EUV emission features

The fundamental Nd:YAG beam was attenuated by varying amounts through the use of polarization optics, allowing for the CE to be evaluated at many different laser intensities, as shown in Figure 2. The dependence of in-band CE for three spot sizes is given for Sn and Li. The planar target geometry emits EUV radiation through a solid angle of 2π steradians. The EUV measurements show that CE is highly dependent on target material, beam intensity, and laser spot size. Our measurements showed that Sn plasma provides a higher CE, reaching peak levels of 2%, as opposed to the Li peak of 1%, which are consistent with previously reported values [8, 9, 25]. The optimal CE achieved is irrespective of the spot sizes used, and is consistent with recent reports of spot size dependence on Sn plasma CE [9]. The peak CE remains constant with varying spot size due to the balance between the lateral expansion-induced energy losses and the re-absorption of the EUV light [9]. Visible emission images obtained with fast imaging clearly showed that with a smaller spot size the plasma expansion is nearly spherical, while with a larger spot size plasma expands cylindrically [26].

A smaller spot size requires a higher intensity to reach the same CE as a large spot size, as seen in Figure 2. For obtaining the highest CE, ideal plasma temperatures and densities should be created for the longest possible period of time with the maximum size. The optimal temperature for in-band EUV production is ~ 30-40 eV. The changes in the spot size will affect the nature of the hydrodynamic expansion and confinement of the plasma [11, 26]. The magnitude of the plasma temperature is provided by a balance between incoming and escaping energy (laser absorption, radiation energy loss, plasma expansion etc.). Recent modeling studies of efficient EUV production at various spot sizes also predicted the requirement of a higher laser intensity for a smaller spot size [11]. In the case of larger laser spots, lower laser intensities are needed for efficient EUV production because of the plasma opacity, and the smaller laser spots create the opposite effect [11]. Hence, the hydrodynamic confinement plays a role in the right shift of CE maxima with smaller spot sizes.

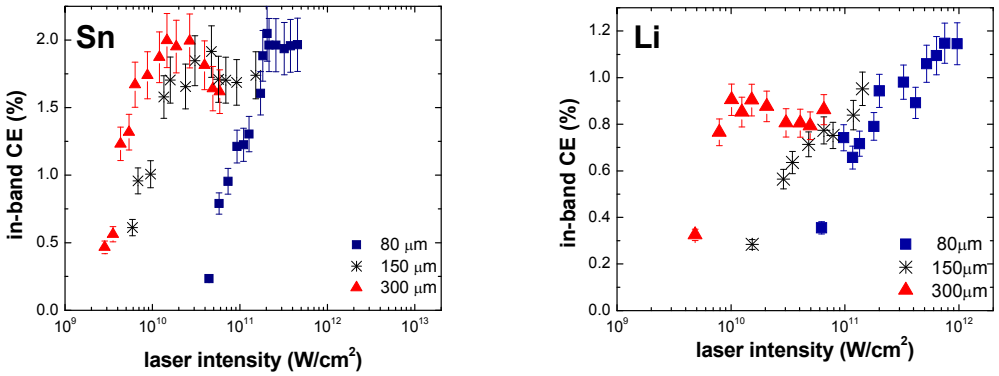

Figure 2. The dependence of conversion efficiency on laser intensity is given for various spot sizes for Sn and Li plasmas.

The saturation, or reduction of the CE, of Sn plasma at higher intensities after reaching the optimal CE could be due to opacity effects. It is known that the dense plasma generated from, and nearby too, a solid Sn target is optically thick to 13.5nm light [27]. However, we noticed CE saturation in Li plasmas as well, especially at larger spot sizes, where the plasma evidently provides a slightly lower CE. For example, Figure 2 shows the estimated maximum CE with a 300 μm spot is 0.8%, while it increased to 1.1% with a 80 μm spot size plasma.

EUV spectral studies are needed to investigate self-absorption properties of Sn and Li plasmas. Several spectra of both materials were recorded with laser pulses of increasing intensity, with a constant spot size of 80 μm, and are given in Figure 3. The EUV emission from the Sn plasma showed a broad-band emission constituted by several ionic stages (commonly called an unresolved transition array (UTA)) [5]. The UTA emission is concentrated around 13.5 nm, with a narrow band gap of 5–10 eV arising from the $4p^6 4d^n - 4p^5 4d^{n+1} + 4p^6 4d^{n-1} 4f$ transitions of various Sn ions, ranging from

Sn^{6+} to Sn^{14+}, with occupancy in transition levels from the range of n = 2 to n = 8 [28]. The main contributors of emission in the in-band region are Sn^{9+}-Sn^{13+} ions. At high laser energies, a spectral dip at the peak of the UTA is very evident, which is mainly due to self-absorption due to opacity effects, as at high intensities the Sn plasma density increases until the plasma becomes optically thick, and reabsorbs the light. Along with the occurrence of a spectral dip, an enhancement in intensity is noted at the higher wavelength side of the UTA with increasing laser intensity. These enhancements are due to recombination effects, where ionized Sn atoms collide with free electrons in the plasma, causing a repopulation of the Sn^{8+}-Sn^{10+} levels, where they strongly radiate outside of in the in-band region[28].

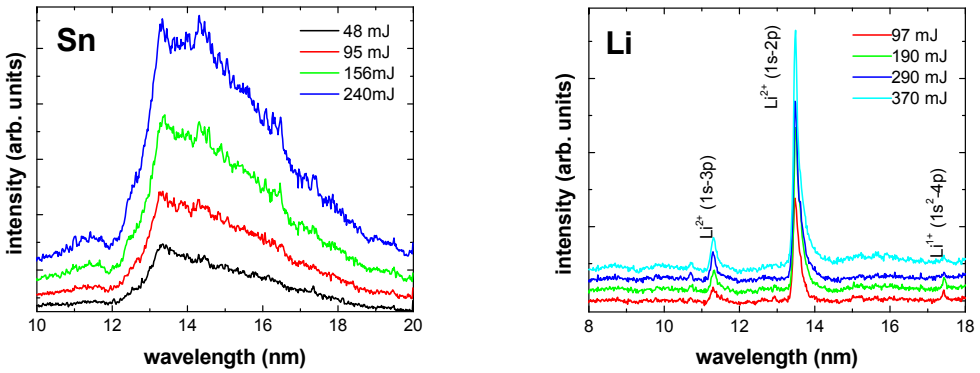

Figure 3. EUV spectral emission features of Sn and Li plasmas. A transmission grating spectrograph with a resolution of 100 ($\lambda/\Delta\lambda$) is used for recording the spectra.

Compared to Sn plasmas, Li plasmas possess discrete line structures. These structures became more intense with increasing laser intensity, but the features themselves remained unchanged. The emission spectra recorded from the TGS shows that the Li^{2+}1s-2p transition (Lyman-α) line at 13.5 nm, as seen in Figure 3, lies completely within the 2% bandwidth of the Mo/Si MLM. It should be mentioned that the transmission grating spectrograph used in the present studies had only a resolution ($\lambda/\Delta\lambda$) of ~ 100; that is not adequate to resolve the finer details in the spectra. However, the effect of spot size on the CE shows the possibility of reabsorption/reheating in the plasma, causing the CE saturation.

We also compared the emission volumes using the images from an EUV filtered pinhole camera, as shown in Figure 4. While the Sn plasma was bright enough to be imaged easily, imaging the Li plasma required taking a multiple-exposure of five separate plasmas. This demonstrates that the EUV emission from the Li plasma were significantly dimmer than those of a Sn plasma at a given laser intensity. This is because our pinhole camera integrates a spectral region from 7-15 nm, an emission region capturing nearly all of the UTA for Sn, but only the Lyman-α line for Li. Plasma aspect ratios were measured from the drop-off from the image's intensity profile peak to $1/e^2$ of that peak value The Li plasma had an aspect ratio of 1.22, and the Sn had a ratio of 1.26. Both plasmas have similar aspect ratios, despite having apparently different shapes.

3.2 Faraday cup ion analysis

In addition to radiating the 13.5 nm in-band light, a LPP will also release debris in the forms of energetic ions (the plasma itself), neutral particles, molten droplets ejected from the ablated target, and out-of-band emission [17]. Ionized and neutral particle flux causes the sputtering and implantation of the debris species into the MLM coating, lowering its reflectivity [20]. In order for the EUVL to be a commercially viable manufacturing technique, the MLMs must last a long time. Several mitigation schemes have been devised to improve MLM lifetime using magnetic fields[6, 22, 29], a gas curtain [17, 21], low-energy pre-pulses [2, 12], and mass-limited targets [10].

The FC is of the simplest methods for analyzing ions from LPPs, but it is a useful tool for obtaining the integrated ion flux, and ion velocity, and thus, the kinetic energy distribution. Typical ion emission and kinetic energy profiles obtained from Sn and Li plasma measure with the FC are given in Figure 5. In these measurements the laser had an intensity of 2 $x10^{11}$ W/cm^2, with a spot size of 80 μm. The ion TOF profile is represented by a sharp prompt peak, followed by a broad

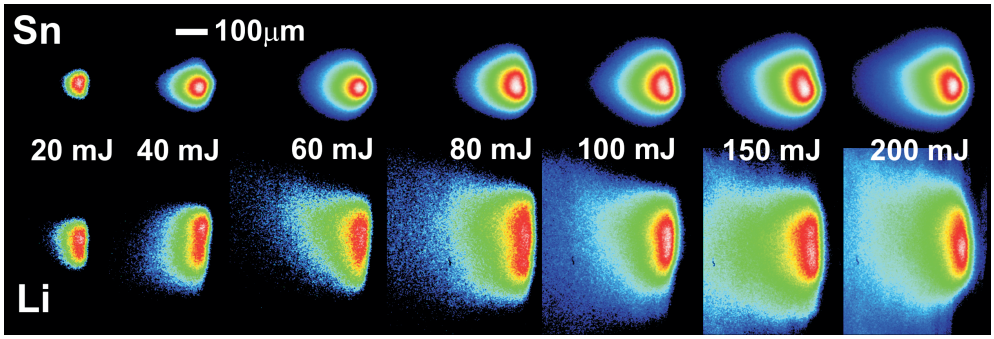

Figure 4. Images of Li and Sn plasmas. False-color has been added to the images to show relative intensities. The Li plasma images are multiple exposures of 5 pulses, and the Sn plasma images are of a single pulse.

slower peak. The fast prompt peak in the ion signal is due to the photoelectric effect, and can be used as a time marker. It is very evident from the figure that Li ions possess a narrower kinetic profile compared to Sn ions. The estimated peak expansion velocities are 4.2±0.2 x10^6 cm/s for Sn ions, and 1.4±0.2 x10^7 cm/s for Li ions. However, due to their lower mass, the kinetic energy of the Li ions is considerably lower compared to the Sn ions. The kinetic energy FWHM spread of Sn ions was found to be 5X greater compared to Li ions at the laser intensity of 2 x10^{11} W/cm^2. Under these intensity conditions, the average charge state <Z> of Sn plasma [24] should be ≥ 11, and ≥ 2 for Li. However, the plasma ions undergo three-body recombination while adiabatically expanding towards the detector. This three-body recombination is proportional to $Z^3T_e^{-9/2}$, where T_e is the plasma temperature. This implies that Li atoms are less prone to recombination.

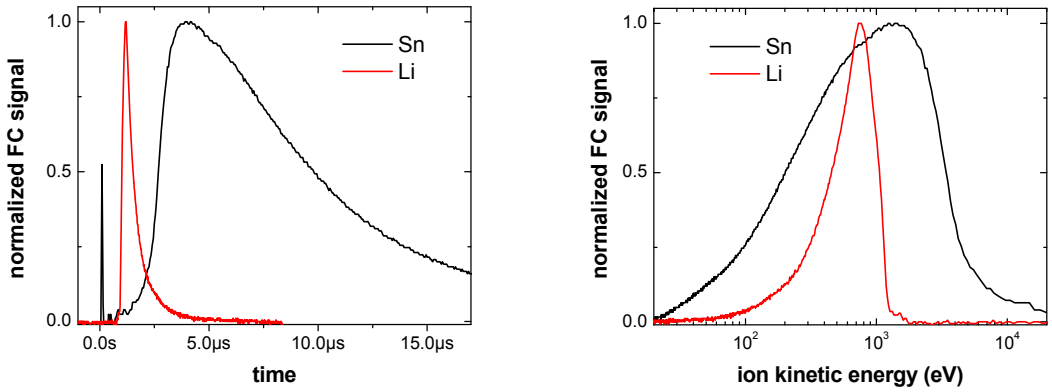

Figure 5. Typical ion profiles recorded with a FC is given for Sn and Li plasma. For these measurements the FC is positioned at 17 cm from the target at an angle 12º. The laser intensity used in this measurement is 2x10^{11} W/cm^2. The kinetic distribution obtained from the time-of-flight ion signal is given in the right figure.

The maximum probable kinetic energies, as well the ion flux of Sn and Li plasmas, depend on laser intensities, as shown in Figure 6. For both Li and Sn plasmas, both the maximum probable kinetic energy and ion fluence showed an exponential decay trend. The reduction in the increasing rate of the kinetic energies and ion fluxes at higher laser intensities could be due to plasma shielding and absorption. Previous studies with identical laser intensities [2] for Sn plasmas clearly showed the plasma could already be at the critical density for the pump beam wavelength. Once the plasma reaches the critical density, the remaining part of the laser pulse interacts with the plasma rather than the target material, effectively reducing the ion flux. The saturation of ion kinetic energy can also be related to the CE measurement, where we also noticed a similar saturation at higher intensities.

Comparing the ion flux and kinetic energies of Sn and Li plasma, one can notice that the peak kinetic energies are always higher for Sn plasma, which could make them more deleterious for MLM mirrors. These results showed that implementing charged particle debris mitigation techniques (electric or magnetic field) is much easier for Li plasma.

However, FC studies showed that although they are less energetic, the ion fluence is significantly higher for Li plasma compared to Sn plasma.

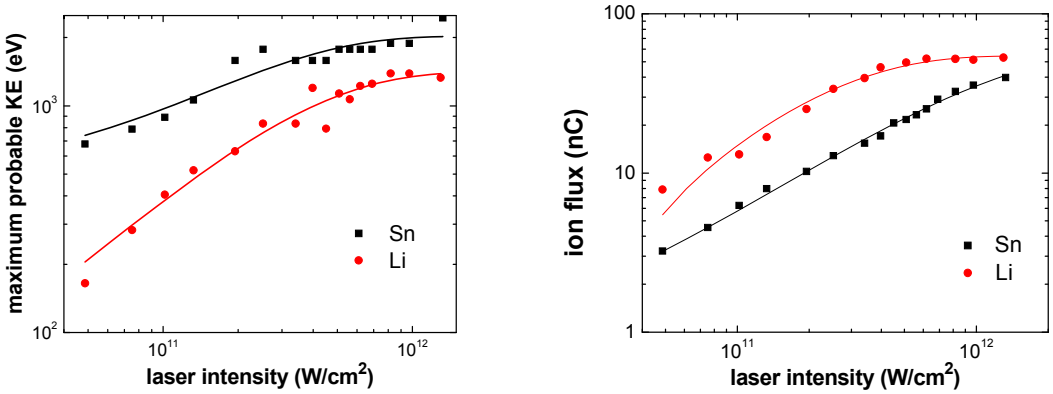

Figure 6. Maximum probable kinetic energies of Sn and Li plasma and ion flux as a function of laser intensity. The smooth curves represent the best fit to the data.

4. CONCLUSIONS

We compared the EUV and visible emissions, and ion debris features, of Nd:YAG laser generated Sn and Li plasmas. The conversion efficiency of the EUV radiation has been shown to strongly depend on laser spot size, laser intensity, and target composition. The Sn plasma reached a peak CE of 2%, and Li CE peaked at 1%. These peak CE values have been found to be independent of spot size, though the two materials reach their peaks at different intensities. The laser intensity required for the optimal CE value was found to be inversely proportional to the laser spot size. The observed saturation or reduction of CE in plasmas at higher intensities could be due to opacity effects. EUV spectral studies of Sn and Li plasmas created by pulses of varying intensity were performed to characterize self-absorption. The EUV emission of Sn plasma showed a broad-band UTA emission concentrated around 13.5 nm, due to emissions from the Sn^{9+}-Sn^{13+} transitions. At high laser energies, a spectral dip at the UTA peak appears due to self-absorption. An enhancement in spectral intensity also appears at the higher wavelength side of the UTA with increasing laser intensity, due to recombination effects. Li plasmas possess discrete line structures (primarily, the Lyman-α line), which became more intense with increasing laser intensity without changing the spectral features. An EUV-filtered pinhole camera showed that the plasma plumes appear to take on different shapes, but have similar aspect ratios.

FC analysis of Sn and Li plasma ion emission was used to generate ion and kinetic energy profiles. Li ions exhibit a much narrower kinetic profile than Sn ions, but the less massive Li ions have a considerably lower kinetic energy than the Sn ions. The plasma ions undergo three-body recombination as they expanded towards the FC, which implied that Li atoms are less prone to recombination. The maximum probable kinetic energies and ion flux of Sn and Li plasmas depends on the laser intensity, and display an exponentially decaying trend. Sn plasmas are found to be more damaging to MLMs due to their higher peak kinetic energies. The Li plasmas demonstrate greater ion fluence, but their lower energies would allow an easier implementation of electromagnetic charged particle debris mitigation systems.

ACKNOWLEDGEMENTS

This work was partially funded by the College of Engineering, Purdue University.

REFERENCES

[1] V. Bakshi, [EUV sources for lithography] SPIE press, New York (2006).
[2] Y. Tao, M. S. Tillack, S. S. Harilal *et al.*, "Investigations on the interaction of a laser pulse with a preformed Gaussian Sn plume for an extreme ultraviolet lithography source," J. Appl. Phys., 101, 023305 (2007).

[3] U. Stamm, "Extreme ultraviolet light sources for use in semiconductor lithography - state of the art and future development," J. Phys. D, 37(23), 3244-3253 (2004).
[4] S. S. Harilal, R. W. Coons, P. Hough *et al.*, "Influence of spot size on extreme ultraviolet efficiency of laser-produced Sn plasmas," Appl. Phys. Lett., 95, 221501 (2009).
[5] J. White, P. Dunne, P. Hayden *et al.*, "Optimizing 13.5 nm laser-produced tin plasma emission as a function of laser wavelength," Appl. Phys. Lett., 90(18), 181502 (2007).
[6] S. S. Harilal, M. S. Tillack, B. O'Shay *et al.*, "Extreme ultraviolet spectral purity and magnetic ion debris mitigation with low density tin targets," Opt. Lett., 31(10), 1549-1551 (2006).
[7] N. Bowering, M. Martins, W. N. Partlo *et al.*, "Extreme ultraviolet emission spectra of highly ionized xenon and their comparison with model calculations," J. Appl. Phys., 95(1), 16-23 (2004).
[8] T. Higashiguchi, K. Kawasaki, W. Sasaki *et al.*, "Enhancement of extreme ultraviolet emission from a lithium plasma by use of dual laser pulses," Appl. Phys. Lett., 88(16), 161502 (2006).
[9] Y. Tao, S. S. Harilal, M. S. Tillack *et al.*, "Effect of focal spot size on in-band 13.5 nm EUVemission from laser-produced Sn plasma," Opt. Lett., 31(16), 2492-2494 (2006).
[10] S. S. Harilal, B. O'Shay, M. S. Tillack *et al.*, "Spectral control of emission from tin doped targets for extreme ultraviolet lithography," J. Phys. D, 39, 484-487 (2006).
[11] A. Hassanein, V. Sizyuk, T. Sizyuk *et al.*, "Effects of Plasma Spatial Profile on Conversion efficiency of Laser-Produced Plasma Sources for EUV lithography," J. Micro/Nanolith. MEMS MOEMS, 8(4), 041503 (2009).
[12] Y. Tao, M. S. Tillack, S. S. Harilal *et al.*, "A mass-limited Sn target irradiated by dual laser pulses for an extreme ultraviolet lithography source," Opt. Lett., 32, 1338-1340 (2007).
[13] S. Yuspeh, K. L. Sequoia, Y. Tao *et al.*, "Optimization of the size ratio of Sn sphere and laser focal spot for an extreme ultraviolet light source," Appl. Phys. Lett., 93(22), 221503 (2008).
[14] S. A. George, W. T. Silfvast, K. Takenoshita *et al.*, "Comparative extreme ultraviolet emission measurements for lithium and tin laser plasmas," Opt. Lett., 32(8), 997-999 (2007).
[15] A. Nagano, T. Inoue, P. E. Nica *et al.*, "Extreme ultraviolet source using a forced recombination process in lithium plasma generated by a pulsed laser," Appl. Phys. Lett., 90(15), 151502 (2007).
[16] Y. Ueno, T. Ariga, G. Soumagne *et al.*, "Efficient extreme ultraviolet plasma source generated by a CO2 laser and a liquid xenon microjet target," Appl. Phys. Lett., 90(19), 191503 (2007).
[17] S. S. Harilal, B. O'Shay, Y. Tao *et al.*, "Ion debris mitigation from tin plasma using ambient gas, magnetic field and combined effects," Appl. Phys. B, 86, 547-53 (2007).
[18] M. J. Neumann, M. Cruce, P. Brown *et al.*, "Effect of deposition, sputtering, and evaporation of lithium debris buildup on EUV optics - art. no. 65172Y," Proc. SPIE, 6517, Y5172-Y5172 (2007).
[19] H. Tanaka, Y. Hashimoto, K. Tamaru *et al.*, "Behavior of debris from laser-produced plasma for extreme ultraviolet light source measured by laser imaging technique," Appl. Phys. Lett., 89(18), 181109 (2006).
[20] J. P. Allain, M. Neito, M. R. Hendricks *et al.*, "IMPACT: a facility studying the interaction of low-energy intense charged particle beams with dynamical hetrogeneous surfaces," Rev. Sci. Instrum., 78, 113105 (2007).
[21] S. Bollanti, F. Bonfigli, E. Burattini *et al.*, "High-efficiency clean EUV plasma source at 10-30 mn, driven by a long-pulse-width excimer laser," Appl. Phys. B, 76(3), 277-284 (2003).
[22] Y. Ueno, G. Soumagne, A. Sumitani *et al.*, "Reduction of debris of a CO2 laser-produced Sn plasma extreme ultraviolet source using a magnetic field," Appl. Phys. Lett., 92(21), 211503 (2008).
[23] S. S. Harilal, J. J. MacFarlane, I. E. Golovkin *et al.*, "Modeling of EUV emission and conversion efficiency from laser-produced tin plasmas for nanolithography - art. no. 692133," Proc. SPIE, 6921, 92133 (2008).
[24] J. White, P. Dunne, P. Hayden *et al.*, "Simplified one-dimensional calculation of 13.5 nm emission in a tin plasma including radiation transport," J. Appl. Phys., 106, 113303 (2009).
[25] T. Ando, S. Fujioka, H. Nishimura *et al.*, "Optimum laser pulse duration for efficient extreme ultraviolet light generation from laser-produced tin plasmas," Appl. Phys. Lett., 89(15), 151501 (2006).
[26] S. S. Harilal, "Influence of spot size on propagation dynamics of laser-produced Sn plasma," J. Appl. Phys., 103, 123306 (2007).
[27] S. Fujioka, H. Nishimura, K. Nishihara *et al.*, "Opacity effect on extreme ultraviolet radiation from laser-produced tin plasmas," Phys. Rev. Lett., 95(23), 235004 (2005).
[28] J. White, A. Cummings, P. Dunne *et al.*, "Simplified calculation of nonlocal thermodynamic equilibrium excited state populations contributing to 13.5 nm emission in a tin plasma," J. Appl. Phys., 101(4), 043301 (2007).
[29] V. Sizyuk, and A. Hassanein, "Modeling and optimization of debris mitigation systems for laser and discharge-produced plasma in EUV lithography devices," J. Micro/Nanolith. MEMS MOEMS, 6(4), 043003 (2007).